

Towards Trapped-Ion Thermometry Using Cavity-Based EIT

Abhijit Kundu,¹ Vijay Bhatt,¹ and Arijit Sharma^{1,2,*}

¹*Department of Physics, Indian Institute of Technology Tirupati, Yerpedu-517619, Andhra Pradesh, India.*

²*Center for Atomic, Molecular, and Optical Sciences and Technologies,
Indian Institute of Technology Tirupati, Yerpedu-517619, Andhra Pradesh, India.*

(Dated: March 27, 2026)

We present a technique for measuring ion temperature using cavity-based electromagnetically induced transparency (EIT) applicable for cavity QED systems. This method enables efficient extraction of the ion's phonon occupation number following sub-Doppler cooling close to the motional ground state. The proposed method requires operation in the resolved-sideband regime, where individual motional states can be selectively addressed for all relevant transitions either by selecting appropriate energy levels for the three-level system or by employing strong confinement with high secular frequencies ($\sim 10MHz$). It relies on monitoring the cavity probe transmission while scanning the probe laser frequency to establish cavity-induced EIT using a control beam, thereby significantly simplifying the measurement procedure. We establish a theoretical model that demonstrates the influence of the thermal state of the trapped ion vis-à-vis the EIT linewidth measured. We show through numerical simulations how the cavity-induced EIT transmission may be used as a thermometry tool to deduce the ion temperature as well as its motional state in the sub-Doppler cooling regime, even for systems that are in the weak coupling regime.

I. INTRODUCTION

Trapped ions offer a well-controlled platform for precision metrology, cavity quantum electrodynamics (QED), and quantum information processing owing to their long coherence time along with an exceptional degree of experimental controllability [1–4].

With successful demonstrations across a wide range of ion species and trapping architectures, resolved sideband cooling has become the workhorse for preparing trapped ions close to the motional ground state [5–7]. Achieving and verifying near-ground-state cooling is of central importance, as even a small residual motional excitation can introduce decoherence and significantly reduce the fidelity of quantum operations [7, 8]. Consequently, precise thermometry following sideband cooling is essential for accurately characterizing the cooling performance and validating the initialization of the motional state prior to subsequent quantum manipulations.

Accurate knowledge of the ion temperature also plays a crucial role in several aspects of trapped-ion quantum technologies. In quantum

information processing, precise thermometry helps mitigate motional decoherence and improves the fidelity of entangling gate operations [9, 10]. In ion-trap experiments, it enables the characterization of anomalous heating rates and provides insight into noise sources that limit trap performance [8]. Furthermore, in cavity-QED based quantum network protocols, controlling and diagnosing the motional state of ions is vital for optimizing ion–photon interfaces and ensuring efficient quantum state transfer between stationary and flying qubits [11, 12].

Post compensation of excess micromotion, the motion of an ion confined in a radio-frequency Paul trap can be described as a simple harmonic oscillator with discrete, equally spaced energy levels, which define the motional states [7]. Ion temperature is directly determined by a discrete phonon occupation number that characterizes the motional state. Determining this phonon occupation provides a crucial benchmark for coherent quantum operations and enables a direct evaluation of the ions' thermal state [1, 7, 13].

A variety of techniques have been developed to deduce the motional occupation of trapped ions [13–15]. The most popular method is resolved sideband thermometry, which assumes

* arijit@iittp.ac.in

a thermal motional distribution and uses the ratio of red to blue sideband transition strengths to estimate the mean phonon occupation [5, 16]. More generally, reconstruction techniques that do not strictly rely on thermal assumptions are made possible by extracting phonon distribution information from Rabi oscillations in carrier and sideband transitions [13–15]. These methods are well known and typically require precise internal-state preparation and the detection of projective states.

Over the past few decades, following the seminal works of Kimble [17], Haroche [18] and Rempe [19], there has been growing interest in cavity-QED with trapped ions due to its potential for the realization of scalable quantum networks, enhanced light-matter coupling, and effective ion-photon interfaces for quantum information processing schemes and applications [20–26]. Interference-based phenomena such as cavity-assisted electromagnetic-induced transparency (EIT) are made possible by the presence of an optical cavity, which alters the interaction between the ion and the electromagnetic field. Since its discovery, EIT [27] has made it possible for a wide range of coherent optical control applications, such as slow light in atomic medium [28], quantum memory [29], laser cooling [30], precision spectroscopy, and sensing [20].

Cavity-based EIT has been studied in a number of regimes to enable features such as narrowing of the cavity linewidth and enhanced optical nonlinearities [23, 24, 31]. A key feature of cavity-induced EIT is its sensitivity to decoherence mechanisms in the coupled ion-cavity system. Coupling to vibrational sidebands causes phonon-dependent dephasing of the effective Λ -type system in the presence of motional excitation, changing the coherence and altering the EIT interference [30, 32]. The cavity-EIT transparency window is thus systematically expanded by thermal phonons. This sensitivity suggests that the cavity-EIT spectrum can provide a spectroscopic signature of the ion’s motional temperature.

Temperature measurements of trapped ions are often performed using resolved-sideband thermometry, which can obtain sensitivity close to the single-phonon level near the motional ground state, as discussed in [1]. Ion temperatures in the $10^{-1} - 10^2$ mK range have also been measured with sub-mK resolution using dark-resonance thermometry, as shown in [33]. In trapped-ion systems imaging-based spatial thermometry typically offers precision at the millikelvin level [34]. Recently, cavity-based thermometry has been proposed, where the ion temperature is inferred from the sensitivity of the cavity emission to the ion’s spatial motion within the cavity mode [4]. In this method, the thermometry is based on a position-dependent cavity coupling resulting from the ions thermal motion.

In contrast, the thermometry scheme proposed in this article depends on the effective Rabi frequency in a cavity-EIT configuration being modified in a phonon-number dependent manner, which causes a detectable shift in the EIT linewidth. As an alternative thermometry method, particularly suited for cavity-QED experiments, our proposed method relies on measuring the cavity transmission spectrum with high frequency resolution. This enables even minute linewidth variations to correspond to discernible temperature changes.

In this article, we theoretically investigate a cavity-enhanced thermometry scheme for trapped ions that exploits the phonon-induced modification of cavity-induced EIT. We consider a Λ -type trapped ion cavity-QED system in which an auxiliary internal transition of the ion is driven by a coupling (control) laser and the cavity mode is interacted with a weak probe field. By including vibrational sidebands and the ion’s motion coupled to a thermal reservoir in a Λ -type ion-cavity setup, we demonstrate that the phonon occupation of the trapped ion modifies the cavity EIT linewidth in a systematic manner. This dependence can be used as a direct probe of the mean phonon number by tuning the coupling field to motional sideband

transitions. Thus, the suggested method offers a cavity-compatible thermometry technique that does not depend on projective state detection after sideband cooling. Our theoretical framework establishes a direct link between measurable modification of the cavity-EIT resonance and motional decoherence induced by thermal phonon. The proposed approach provides an experimentally feasible alternative to conventional sideband thermometry in trapped-ion cavity-QED systems.

We show that the coupling laser causes a phonon number-dependent change in the effective Rabi frequency when it is tuned to a motional sideband transition. This results in a systematic and temperature-dependent broadening of the cavity-EIT feature. We determine a quantitative relationship between the measured cavity-EIT linewidth and the ion temperature by numerically solving the complete open-system dynamics, which includes cavity loss, spontaneous emission, and phonon damping caused by a thermal reservoir. Our results indicate that this technique allows for precise thermometry in the resolved-sideband and sub-Doppler regimes and can be expanded to parameter regimes that are consistent with experimentally realized strong coupling ion-cavity systems[23–26].

We subsequently extend the model to the multi-ion system by modifying the atom-cavity interaction Hamiltonian to include a summation over all ions coupled to the same cavity mode. In this formulation, each ion interacts with the cavity field identically, and the collective response of the ion ensemble naturally emerges from the full many-body master equation. This approach allows us to examine thermometry in regimes where the cavity response is strengthened by the collective light-matter interaction inspite of the single-ion coupling strength to the intracavity field placing the system in the weak coupling regime.

To summarize, we establish a direct link between motional decoherence and cavity

transmission, and propose a cavity-compatible minimally invasive thermometry technique for trapped ions through modeling and simulations. Beyond thermometry, the demonstrated sensitivity of cavity-EIT to the motional state of the ion creates new opportunities for studying measurement-induced back-action in cavity-QED systems and for monitoring of thermal dynamics.

The article is structured as follows: In section II, we demonstrate the theoretical model and Hamiltonian, including the treatment of ion motion and dissipative processes. In section III, numerical results for linewidth extraction and cavity transmission are shown. section IV examines how phonons affect the cavity-EIT spectrum. The analysis of ion temperature and the role of thermalization dynamics are discussed in section V. The discussion then extends to multi-ion cavity-QED systems operating in the weak single-ion coupling regime in section VI, where we demonstrate that thermometry is made possible even in cases where individual coupling strengths are small through collective enhancement. section VII further investigates the applicability of the proposed method to systems with large excited state decay rates. We show conclusively that thermometry remains feasible under realistic experimental conditions. In section VIII, we evaluate the projected sensitivity of the thermometry method. We present a realistic experimental realization roadmap in section IX covering parameter regimes compatible with existing ion-cavity platform trap requirements and viable cavity configurations. Finally, section X summarizes the main findings of this work and presents the concluding remarks.

II. THEORY AND MODEL

Cavity-based EIT systems have been extensively studied over the past two decades [23, 24, 31, 35–39]. These studies demonstrate that the cavity output can be effectively controlled by several key parameters, including the control-field Rabi frequency (Ω_c), the atom-

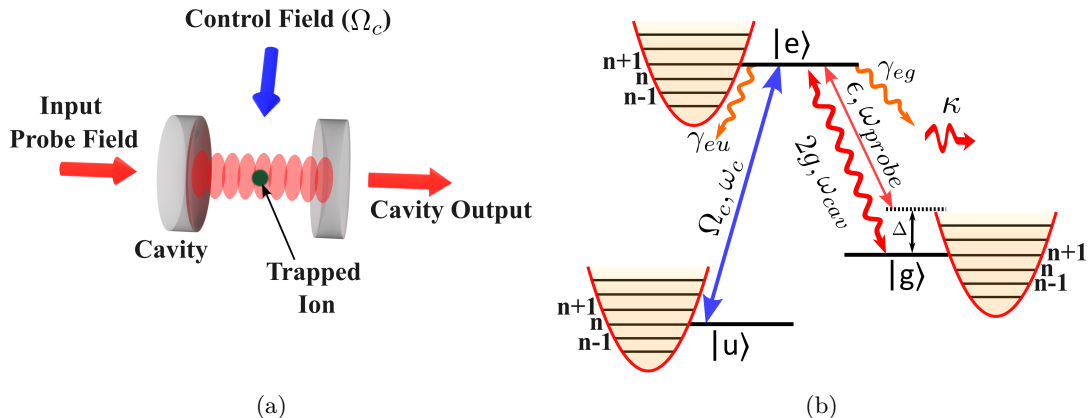


FIG. 1: (a) Schematic of the cavity-based electromagnetically induced transparency (EIT) configuration, where a trapped ion interacts with a single cavity mode. (b) Energy-level diagram of the cavity-EIT scheme including vibrational states. The coupling laser drives the $|u\rangle \rightarrow |e\rangle$ transition with the addition of one vibrational quantum, while spontaneous decay to $|g\rangle$ preserves the vibrational level. The probe field and cavity mode couple the $|e\rangle$ and $|g\rangle$ states.

cavity coupling strength (g), and the cavity decay rate (κ). Among these parameters, Ω_c represents an experimentally accessible degree of freedom, whereas the others are primarily defined by the cavity geometry, mirror reflectivity, and the choice of atomic energy levels. As a result, parameters such as g and κ cannot be easily tuned under typical experimental constraints, whereas Ω_c can be easily modified by tweaking the laser power. As Ω_c increases, the full width at half maximum (FWHM) of the EIT resonance also increases significantly, typically by ≈ 10 kHz. This dependence forms the basis of the proposed thermometry scheme.

For the purpose of ion thermometry, it is essential to include the vibrational levels associated with each relevant electronic energy level. Addressing these vibrational states requires operation in the resolved-sideband regime ($\gamma \ll \omega_{sec}$) [1, 40], where the splitting between adjacent vibrational levels, $\hbar\omega_{sec}$, exceeds the natural linewidth of the corresponding transition, 2γ . Here, ω_{sec} represents the secular frequency of the trapped ion, and γ denotes the spontaneous decay rate of the transition.

Henceforth, a transition between two energy

levels refers to a transition between their corresponding vibrational states. The allowed transitions can be classified into three main types: the red sideband (RSB) transition, the blue sideband (BSB) transition, and the carrier transition, corresponding to $\Delta n = \mp 1$ and $\Delta n = 0$, respectively. The vibrational level occupancy, n , directly influences the ion-field coupling strength when sideband transitions are addressed. Consequently, the Rabi frequencies for the RSB and BSB transitions get modified as [1],

$$\begin{aligned}\Omega_{BSB} &= \Omega_0 \sqrt{n+1}, \\ \Omega_{RSB} &= \Omega_0 \sqrt{n}.\end{aligned}\quad (1)$$

Unlike the previous case, the Rabi frequency (Ω_0) remains unchanged for the carrier transition. Thus, when the control laser is tuned to the BSB or RSB transition, the effect of the phonon occupancy, n , becomes evident in the EIT linewidth through its influence on the Rabi frequency, Ω_c . In other words, variations in the EIT linewidth provide an estimate of changes in the ion's vibrational occupancy. Motivated by this correlation, we define a systematic approach via numerical simulations for determining the ion temperature via phonon occupancy.

We consider a Λ -type three-level system placed

inside a high-finesse optical cavity. The states are considered to be coupled with vibrational states, denoted by $|u, n\rangle$, $|e, n+1\rangle$, and $|g, n\rangle$. The cavity mode interacts with the atomic transition $|g, n+1\rangle \leftrightarrow |e, n+1\rangle$ with coupling strength g , while a classical control laser couples the transition $|u, n\rangle \leftrightarrow |e, n+1\rangle$ by a change in single quanta of the phonon mode with Rabi frequency Ω_c (see Figure 1b). A weak input probe field of amplitude ϵ and frequency ω_{probe} is applied at probe detuning (Δ). To obtain the cavity output, the Δ is scanned on both side of the cavity resonance. The spontaneous emission rates from level $|e, n+1\rangle \rightarrow |u, n+1\rangle$ and $|e, n+1\rangle \rightarrow |g, n+1\rangle$ are γ_{eu} and, γ_{eg} respectively.

We operate in the Lamb-Dicke regime ($\eta \ll 1$), where the control laser and ion's motion can be expanded to first order in the Lamb-Dicke parameter η . Operators b and b^\dagger describe phonon-assisted transitions, achieved by tuning the coupling laser to the first motional sideband of the $|u\rangle \leftrightarrow |e\rangle$ transition [1].

In the rotating frame defined by the probe frequency ω_{probe} , the dynamics of the system can be described by the following time-independent Hamiltonian under the electric dipole and rotating-wave approximation (RWA) (with $\hbar = 1$):

$$H = \Delta_p \sigma_{gg} - \Delta_p a^\dagger a + g (a^\dagger \sigma_{ge} + a \sigma_{eg}) + \eta \Omega_c (\sigma_{eu} b^\dagger + \sigma_{ue} b) + \epsilon (a^\dagger + a). \quad (2)$$

Here, $\sigma_{ij} = |i\rangle \langle j|$ are the ionic transition operators. The detuning parameter $\Delta_p = \omega_{probe} - \omega_{31}$ represents the frequency mismatch between the probe laser and the atomic transition $|g, n+1\rangle \leftrightarrow |e, n+1\rangle$.

The first term of the Hamiltonian in Equation 2 describes the energy of the state $|g, n+1\rangle$ in the rotating frame, while the second term corresponds to the energy of the cavity photons. The cavity field is represented using the photon annihilation (a) and creation (a^\dagger) operators.

The third term of the Hamiltonian in Equation 2 accounts for the coherent interaction between the cavity field and the atomic transition $|g, n+1\rangle \leftrightarrow |e, n+1\rangle$. The fourth term describes the interaction between the atomic transition $|e, n+1\rangle \leftrightarrow |u, n+1\rangle$ and the vibrational mode of the ion, mediated by the control laser. Here, b^\dagger and b are the phonon creation and annihilation operators respectively. The last term represents the coherent drive applied to the cavity field by the pump laser.

The open dynamics follow the Lindblad master equation [41],

$$\begin{aligned} \frac{d\rho}{dt} = & -i[H, \rho] + \kappa (2a\rho a^\dagger - a^\dagger a \rho - \rho a^\dagger a) \\ & + \gamma_{eu} (2\sigma_{ue}\rho\sigma_{eu} - \sigma_{ee}\rho - \rho\sigma_{ee}) \\ & + \gamma_{eg} (2\sigma_{ge}\rho\sigma_{eg} - \sigma_{ee}\rho - \rho\sigma_{ee}) \\ & + \gamma_b (n_{th} + 1) (2b\rho b^\dagger - b^\dagger b \rho - \rho b^\dagger b) \\ & + \gamma_b n_{th} (2b^\dagger \rho b - b b^\dagger \rho - \rho b b^\dagger) \end{aligned} \quad (3)$$

where ρ represents the density matrix of the ion-cavity system and κ denotes the decay rate of the cavity field. γ_{eg} and γ_{eu} represent the spontaneous decay rate from state $|e\rangle$ to state $|g\rangle$ and $|u\rangle$. γ_b is the phonon damping rate and n_{th} denotes the mean thermal phonon number at equilibrium.

The average phonon number (\bar{n}) is related to the temperature of the ion as,

$$\bar{n} = \frac{1}{\exp(\hbar\omega_{osc}/k_b T) - 1} \quad (4)$$

The phonon states are inherent to damping due to fluctuating electric field noise present in real ion trap. To account for this scenario, we considered the trapped ion system such that it is coupled to a thermal bath. Fluctuating electric-field noise induces phonon exchange between the ion and its surrounding reservoir, driving the system towards thermal equilibrium [8].

The rate equation for the phonons can be derived as [8],

$$\dot{\bar{n}}(t) = -\gamma_b \bar{n}(t) + \gamma_b n_{th} \quad (5)$$

so close to the ground state ($\bar{n} = 0$), $\dot{\bar{n}}(t) = \gamma_b n_{th}$. This gives an initial estimation of the heating rate of the ion. Equation 5, also shows that if a long time interval is taken, i.e., at equilibrium, $\bar{n}_{eq} = n_{th}$. So, determining the value of n_{th} provides an estimate of the ion temperature owing to Equation 4.

III. ANALYSIS OF TRANSMISSION IN CAVITY-EIT

To study the system dynamics, the master equation (Equation 3) has been solved numerically using the Hamiltonian given in Equation 2 for a single ion strongly coupled to the intracavity field. The probe laser frequency is scanned across the cavity resonance, keeping the other system parameters fixed. The steady-state density matrix is obtained for each value of the probe detuning.

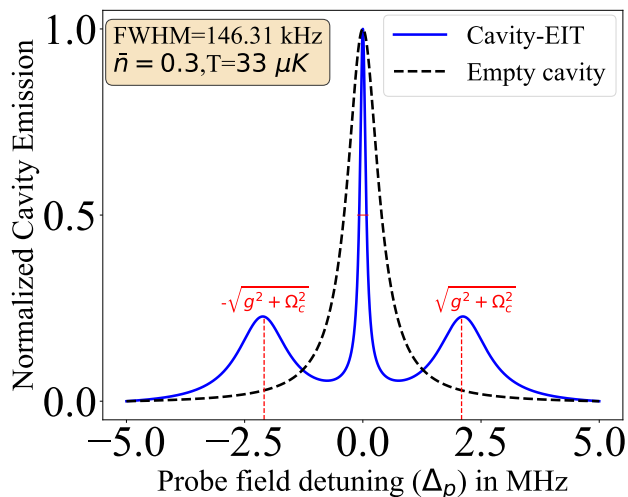


FIG. 2: Simulated cavity-EIT transmission spectrum for $\kappa = 0.4$ MHz, $g = 5\kappa$, $\gamma_{eg} = \gamma_{eu} = \kappa$, $\bar{n} = 0.1$, and $\gamma_b = 0.6\kappa$. The observed linewidth (0.22 MHz) is narrower than the empty cavity linewidth $2\kappa = 0.8$ MHz. The vacuum Rabi splitting peaks occur at $\pm\sqrt{g^2 + \Omega_c^2} = \pm 2.33$ MHz.

From the steady-state solution, the inter-cavity photon population is extracted by

evaluating the expectation value of the photon number operator ($\langle a^\dagger a \rangle$). The steady-state intra-cavity photon number, which is proportional to the output field leaking through the cavity mirrors, is then used to calculate the transmission spectrum. In Figure 2 the resulting transmission profile is illustrated. This spectrum exhibits the characteristic features of previously reported cavity-EIT systems [23, 24, 31, 42].

The cavity linewidth is observed to be narrower than that of an empty cavity, and the vacuum Rabi splitting peaks appear at $\Delta = \pm\sqrt{g^2 + \Omega_c^2}$. For all simulations presented in this work, unless otherwise stated, the system parameters are fixed as follows. All quantities are normalized with respect to the cavity decay rate, κ , which is taken to be 0.4 MHz, a typical value for a high-finesse cavity. The coupling-field Rabi frequency, Ω_c , is set to 2.5κ , while the atom-cavity coupling strength, g , is chosen as 3κ . The decay rates from the excited states, γ_{ge} and γ_{ue} , are taken to be equal to κ . In addition, motional-state decoherence is included to account for unwanted heating or cooling of the ion arising from phase noise and radiative fluctuations present in realistic ion traps. To model this effect, a weak coupling between the motional state and the environment is introduced, characterized by a coupling constant $\gamma_b \approx 0.25\kappa$.

IV. EFFECT OF THERMAL STATE ON CAVITY EIT LINEWIDTH

The usual cavity-EIT formalism discussed and reviewed through multiple theoretical approaches [43–45] as well as experimental investigations [38, 46] till date has not explicitly considered the ion's motional state in the realization of the cavity-induced EIT phenomenon. This inherently makes an assumption that the ion is fixed in space and the effect of ion thermalization does not affect the cavity-EIT output. When the ion's motion is not considered for cavity-based

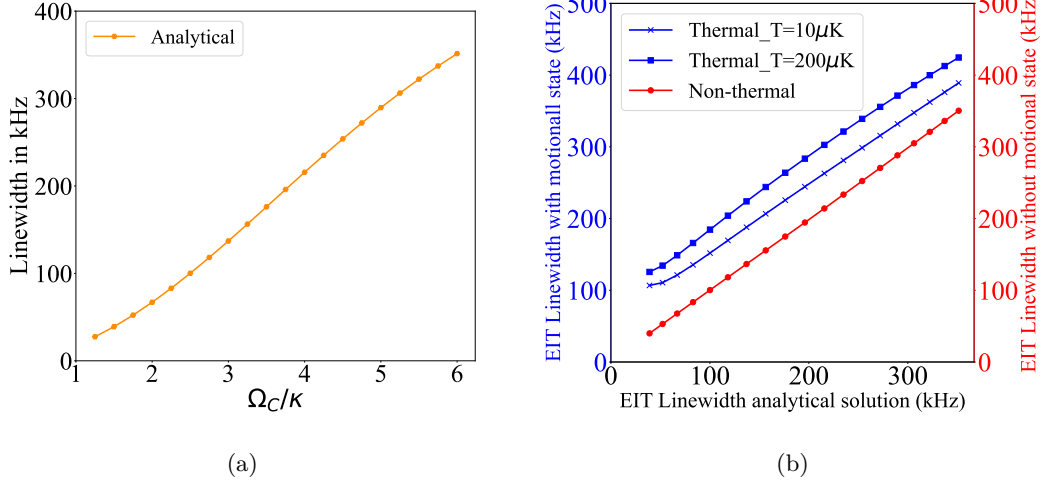


FIG. 3: (a) Cavity-EIT linewidth from analytical expression as a function of control field Rabi frequency. (b) Comparison of linewidth without considering motional state vs with motional state for different temperatures of ion. The parameters for the plots chosen as follows, $\kappa = 0.4\text{MHz}$, $g = 3\kappa$, $\gamma_{eg} = \gamma_{eu} = \kappa$, $\gamma_b = 0.04\kappa$.

EIT, the Hamiltonian is simplified to,

$$H_{\text{EIT}} = \Delta_p \sigma_{gg} - \Delta_p a^\dagger a + g (a^\dagger \sigma_{ge} + \sigma_{eg} a) + \Omega_c (\sigma_{ue} + \sigma_{eu}) + \varepsilon (a^\dagger + a). \quad (6)$$

where the different terms have their usual meaning as described in section II. We refer to this formalism as non-thermal and the Hamiltonian given in Equation 6, the non-thermal cavity-EIT Hamiltonian. The output of the cavity is traced from the average of the photon number operator with the variation of the probe field detuning. The same cavity transmission can also be analytically calculated from the expression[47],

$$T = \frac{\kappa^2}{|(\Delta_p + i\kappa) - g^2 N \chi|^2} \quad (7)$$

where,

$$\chi = g^2 N \frac{\Delta_p}{(\Delta_p + i(\gamma_{eu} + \gamma_{eg})\Delta_p - \frac{1}{4}\Omega_c^2)} \quad (8)$$

The linewidth depends on the effective Rabi coupling, Ω_c , exhibiting power-broadening behavior. In Figure 3a, the relationship between the effective Rabi coupling and the cavity-EIT linewidth is shown using the analytical expression.

When the motional states are incorporated into the Hamiltonian (Equation 10), it encompasses a more general description of a trapped ion, the cavity-EIT linewidth deviates from the non-thermal case. As the temperature increases, the thermal nature of the ion leads to a higher motional occupancy. This increase in motional occupation modifies the cavity-EIT linewidth by changing Ω_c , as discussed in detail in section II.

To compare the cavity-induced EIT linewidths in the thermal (when motional states are included) and non-thermal (when motional states are not considered) cases, we perform simulations for both scenarios using the same values of Ω_c as those employed in the analytical plot in Figure 3a. The thermal simulations are carried out over a range of temperatures to capture the dependence of the cavity-induced EIT linewidth on the ion temperature. In Figure 3b, the thermal and non-thermal linewidths are presented, with the analytical linewidths from Figure 3a used as the reference on the x-axis.

It is shown that, over the entire range, the non-thermal linewidth remains lower than the thermal linewidth and that the linewidth curves shift toward higher values as the temperature increases. This behavior provides further mo-

tivation for quantifying the ion temperature, as it modifies the cavity linewidth, which is highly sensitive to temperature-induced changes in the ion's motional state.

V. DETERMINATION OF ION TEMPERATURE AND AVERAGE PHONON NUMBER

We study the cavity-based EIT phenomenon with the motivation of determining the ion temperature. It is evident from section IV that the linewidth of the cavity-EIT spectrum appears to serve as a probe parameter for the trapped ion temperature. The ion temperature is incorporated in the systems by means of the thermal bath phonon occupancy (n_{th}) following Equation 4 and Equation 5 in steady-state.

The simulation is performed for four different values of the thermal bath phonon occupancy, $n_{th} = 0.5, 1, 5,$ and 10 , using the same set of parameters described in section III. A clear trend of increasing linewidth with increasing n_{th} is observed (see Figure 4a). This behavior indicates that the ion temperature can be mapped to the observed cavity-EIT linewidth. In other words, by analyzing the EIT width of the cavity-EIT spectrum, the ion temperature can be inferred. In the subsequent sections, we discuss the applicability of this technique over a wide range of experimental parameters that govern current and futuristic cavity-QED systems in the strong and weak coupling regimes.

In addition, the average phonon occupancy, \bar{n} , is an important quantity for various applications, such as estimating heating rates [11], determining the fidelity of ion trap-based quantum gates [48], indicating the Lamb-Dicke regime etc [1]. Since the phonon occupancy is directly related to temperature (see Equation 4), \bar{n} can also be estimated from the cavity-EIT linewidth [49].

We further perform simulations over a wide range of ion temperatures, from which the linewidth is calculated by fitting a Lorentzian function to the spectrum. The average phonon occupancy \bar{n} is extracted by taking the expecta-

tion over phonon number operator ($\langle\langle b^\dagger b \rangle\rangle$). In Figure 4b, the ion temperature and \bar{n} are illustrated as functions of the cavity-EIT linewidth. The predicted temperature exhibits an asymptotic behavior at low linewidth values, indicating that at high temperatures, variations in linewidth are minimal.

This behavior can be understood from the $\sqrt{\bar{n}}$ dependence of the control field Rabi frequency, Ω_c , which directly governs the cavity-EIT linewidth. At low temperatures, small changes in temperature lead to rapid variations in Ω_c , as described by Equation 1, resulting in noticeable changes in the linewidth. In contrast, at higher temperatures, the linewidth tends to saturate because variations in Ω_c become negligible.

The average phonon occupation, \bar{n} , follows a similar trend to the temperature as the cavity-EIT linewidth changes. This behavior arises from the approximately linear relationship between \bar{n} and temperature derived from Equation 4, given by

$$\bar{n} \approx \frac{k_B T}{\hbar \omega} \quad (9)$$

Further, we demonstrate how the ion-cavity coupling strength affects the cavity-EIT linewidth, g , and Rabi frequency of the coupling laser. We provide linewidth maps in two dimensions for a range of mean thermal phonon number values. Appendix C contains the relevant discussion and the requisite plots.

VI. THERMOMETRY OF A MULTI-ION CAVITY-QED SYSTEM IN THE WEAK COUPLING REGIME

The discussion so far has focused on a single ion confined in a high-finesse cavity and operating in the strong coupling regime. However, operating in the strong-coupling regime is experimentally challenging with only a single ion, requiring either a near concentric-cavity regime [50] or fiber cavities where the polished surfaces are placed very close to each other [51]. Interestingly, both of these configurations

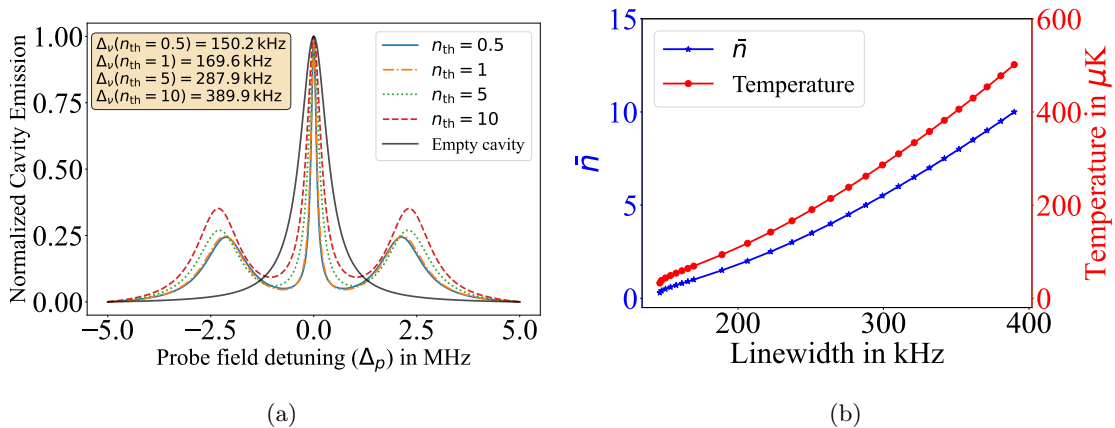


FIG. 4: (a) Cavity-EIT spectrum for different n_{th} value (b) Ion temperature and average phonon occupancy (\bar{n}) as a function of cavity-EIT linewidth. The cavity decay rate, $\kappa = 0.4\text{MHz}$, cavity coupling factor, $g = 5\kappa$. The decay rates from the excited states are taken as $\gamma_{eg} = \gamma_{eu} = \kappa$. The phonon coupling rate is taken as $\gamma_b = 0.6\kappa$.

possess very small mode volumes leading to an increase in the single-atom cooperativity factor in a significant manner. Both regimes of operation are experimentally challenging, with substantial effort necessary in making and aligning cavity mirrors with very high reflectivity for the above two cavity configurations.

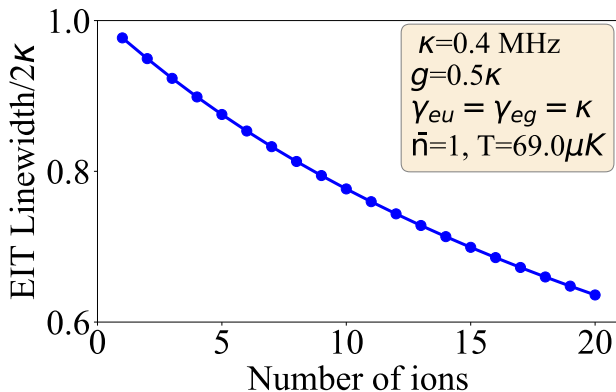


FIG. 5: Cavity-EIT linewidth variation with the number of ions. The simulation parameters are shown in the inset.

Our analysis reveals that it is possible to perform ion thermometry measurements for multi-ion cavity-QED systems having a relatively low single-ion cavity coupling factor ($g \ll \kappa, \gamma$) that places such systems in the weak coupling regime ($g \ll \kappa, \gamma$) for a single ion. We show through numerical simulations that is possible to apply

the proposed cavity EIT-based ion-thermometry method discussed earlier even for such systems in the weak coupling regime, albeit using more than one ion coupled to the cavity mode instead of a single one. Using a multi-ion configuration coupled to the cavity mode places the system effectively in the strong coupling regime due to the collective ($g_{eff} \propto \sqrt{N}$) scaling up of the single-ion cavity coupling factor.

The Hamiltonian for a multi-ion cavity-QED system may be stated as

$$H = \Delta_p S_{gg} - \Delta_p a^\dagger a + g (a^\dagger S_{ge} + a S_{eg}) + \eta \Omega_c (S_{eu} b^\dagger + S_{ue} b) + \epsilon (a^\dagger + a). \quad (10)$$

where,

$$S_{ij} = \sum_{k=1}^{N_{\text{ion}}} |i\rangle^{(k)} \langle j|^{(k)} = \sum_{k=1}^{N_{\text{ion}}} \sigma_{ij}^{(k)}.$$

are the collective raising and lowering ionic operators for $i \neq j$, and ionic energy-level population operators for $i = j$.

The system dynamics, including the decoherence and dissipative effects, are determined by the master equation as,

$$\begin{aligned}
\frac{d\rho}{dt} = & -i[H, \rho] + \kappa \left(2a\rho a^\dagger - a^\dagger a \rho - \rho a^\dagger a \right) \\
& + \gamma_{eu} \sum_{k=1}^{N_{\text{ion}}} \left(2\sigma_{ue}^{(k)} \rho \sigma_{eu}^{(k)} - \sigma_{ee}^{(k)} \rho - \rho \sigma_{ee}^{(k)} \right) \\
& + \gamma_{eg} \sum_{k=1}^{N_{\text{ion}}} \left(2\sigma_{ge}^{(k)} \rho \sigma_{eg}^{(k)} - \sigma_{ee}^{(k)} \rho - \rho \sigma_{ee}^{(k)} \right) \\
& + \gamma_{u,deph} \sum_{k=1}^{N_{\text{ion}}} \left(2\sigma_{uu}^{(k)} \rho \sigma_{uu}^{(k)} - \sigma_{uu}^{(k)} \rho - \rho \sigma_{uu}^{(k)} \right) \\
& + \gamma_b (n_{\text{th}} + 1) \left(2b\rho b^\dagger - b^\dagger b \rho - \rho b^\dagger b \right) \\
& + \gamma_b n_{\text{th}} \left(2b^\dagger \rho b - bb^\dagger \rho - \rho bb^\dagger \right).
\end{aligned} \tag{11}$$

The method works as one may achieve the collective strong coupling regime with a larger number of ions coupled to the cavity mode, thanks to the scaling of the single-atom cavity coupling factor ($g_{eff} \propto \sqrt{N}$) g with ion number, N [52]. Here g is the single-ion cavity coupling factor. The dependence of ion number on cavity-EIT linewidth is depicted in Figure 5. As the ion number increases, the cavity-EIT linewidth decreases exponentially, making the EIT linewidth even narrower than the single-atom case in the strong coupling regime. It suggests that using a sufficient number of atoms/ions collectively coupled to the cavity, one may be able to realize a very narrow cavity-EIT linewidth, which might be useful for a variety of other applications as well, such as using them as reference transitions in atomic clocks, laser frequency stabilization, etc.

In the multi-atom/ion cavity system, the ion-cloud temperature may be estimated in a similar manner as outlined in the single-ion cavity EIT-based thermometry scheme as discussed in section V. In Figure 6, we have shown the variation in temperature as a function of cavity-EIT linewidth in a fraction of empty cavity linewidth for different numbers of ions. The variation of the cavity EIT linewidth with temperature indicates that the linewidth is more sensitive to the temperature as one considers

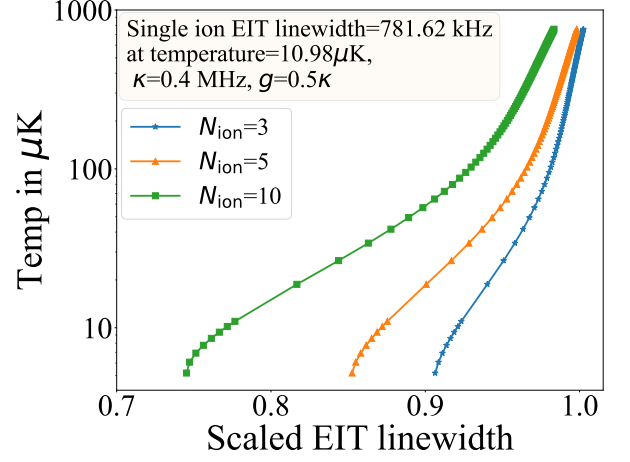


FIG. 6: Temperature vs cavity-EIT linewidth for a multi-ion system. The EIT linewidth is scaled with respect to the empty cavity width. The typical single-ion cavity-EIT linewidth for a chosen temperature is shown in the inset with other system parameters. Except for temperature, the same parameters have been chosen for the simulations performed in this plot.

a higher number of atoms/ions coupled to the cavity mode. Thus, the proposed thermometry method is particularly well-suited for cavity-QED systems with low ion-cavity coupling strength, especially when multiple ions are coupled to the cavity mode.

In the multi-ion model, we assume that all ions share an identical thermal occupation. This approximation is justified under a uniformly cooled condition, where all the ions are cooled to a sufficiently low temperature ($\approx 10 - 50\mu K$) and undergo comparable coupling to the cavity field. Consequently, the collective cavity response can be described using a thermal distribution reminiscent of a single ion.

VII. THERMOMETRY OF A MULTI-ION CAVITY-QED SYSTEM WITH A LARGE EXCITED-STATE DECAY RATE

The three-level system we have considered for our ion thermometry is an ideal system, with a very low decay rate from the excited state. However, most ion species used in trapped-ion experiments have a broad excited-state linewidth (i.e.,

a large decay rate), which helps cool the ions efficiently with Doppler cooling.

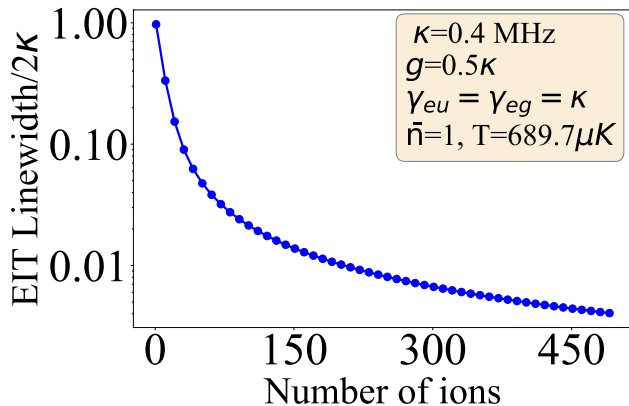


FIG. 7: Variation of cavity-EIT linewidth with the number of ions with large decay rate of ion excited state. The simulation parameters are shown in the inset.

A large decay rate induces decoherence in the system, leading to a negligible cavity-EIT effect, and only the bare cavity signal remains visible at the output. Several groups worldwide have demonstrated the cavity-EIT effect using ion/atom species with a large decay rate from the excited state [23, 52]. The experimental results from these systems show that for a single ion the cavity-EIT signal is not clearly visible; however, increasing the number of atoms/ions coupled to the cavity mode leads to the re-appearance of cavity-EIT spectrum. This occurs because, although the ion-cavity system is not configured in the strong coupling regime for a single ion/atom (as the decay rates far exceed the single atom cavity coupling factor), the effective coupling strength increases with multiple ions coupled to the intracavity field. Consequently, the collective ion-cavity coupling can overcome the large decay rates of the excited states, as discussed in section VI. More discussion about their system and an excellent agreement of our simulation results with the analytical expression and the reported experimental data can be found in Appendix A and B.

Motivated by these studies, we extend our ion-thermometry method to cases where the excited state decays rapidly to the ground states

in a three-level lambda system. The cavity-EIT peaks become visible when considering a multi-ion system, and the linewidth decreases with the increasing number of atoms, which is the usual behavior similar to that obtained in section VI. The variation of the cavity linewidth with the number of atoms, obtained from simulations performed for up to 500 ions, along with the corresponding simulation parameters, is depicted in Figure 7.

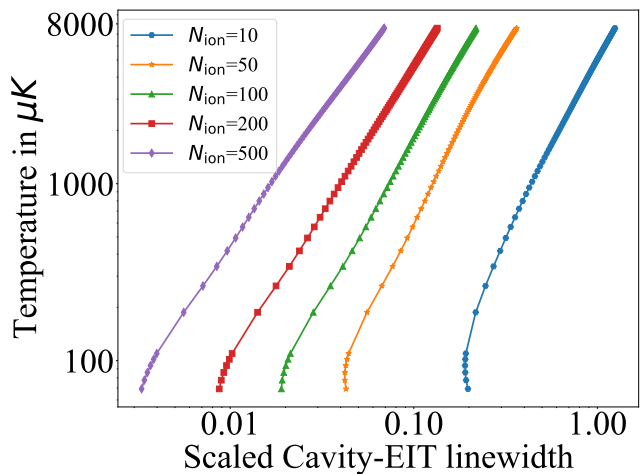


FIG. 8: Temperature vs linewidth for large decay from the excited level. For running the simulation, the cavity decay rate (κ) is taken as $0.4 MHz$, whereas the cavity coupling factor is taken as $g = 3\kappa$. The decay rates from excited state $|e\rangle$ to $|u\rangle$ and $|g\rangle$ are $\gamma_{eu} = 20\kappa$, $\gamma_{eg} = 7\kappa$ respectively. The control field Rabi frequency is chosen as $\Omega_c = 2.5\kappa$, whereas the phonon coupling rate to the phonon bath is taken as $\gamma_b = 0.5\kappa$. The maximum probe field intensity (ϵ/κ) is taken as 0.01. Here, the cavity-EIT linewidth is scaled with respect to the empty cavity linewidth (2κ).

Interestingly, when running the simulations at different temperatures, i.e., for different values of n_{th} , the linewidth does not vary at all. This occurs because, for systems with large decay rates, the resolved sideband condition ($\gamma \ll \omega_{sec}$) is no longer satisfied. As a result, the motional sidebands cannot be resolved, which is essential for the thermometry process. Therefore, we conclude that, in addition to strong coupling, a necessary condition for implementing this thermometry method is that the ion must operate in the resolved sideband

regime. The only remaining option in such cases is to increase the trap frequency ω_c ; in other words, a tighter confinement of the ion with a deeper trapping potential is required.

To assess the applicability of the thermometry method in the presence of an excited state with a relatively large decay rate (> 7 -8 MHz), we analyze the temperature dependence of the cavity-EIT linewidth for different numbers of ions as shown in Figure 8. A distinct and monotonic dependence of the normalized linewidth on the temperature is preserved even for large decay rates ($\gamma_{eu} = 20\kappa$, $\gamma_{eg} = 7\kappa$). Although the decoherence caused by spontaneous emission, which also partially broadens the EIT feature, collective enhancement ($g_{eff} \propto \sqrt{N}$) strengthens the effective light-matter interaction to compensate for decoherence. These results demonstrate that the suggested cavity-EIT thermometry method is robust even in regimes of significant radiative decay.

VIII. PROJECTED SENSITIVITY OF CAVITY-INDUCED EIT THERMOMETRY

As discussed in the previous two sections, our method is applicable to both the weak-coupling regime and to systems with large excited-state decay rates. An important question that might arise pertains to how accurately our proposed technique can sense variations in temperature and what is the potential sensitivity corresponding to the average phonon occupation. Addressing this question provides insight into the practical applicability of the method across different parameter regimes. Furthermore, a sensitivity analysis helps to quantify the precision of the thermometry technique and highlights its strengths as well as its limitations.

From the observations in Figure 6 and Figure 8, it is evident that the variation of the linewidth is not uniform across the entire temperature range. Consequently, the sensitivity of our method depends on the specific temperature regime under consideration. To quantify this behavior, we define the temperature sensitivity as

the change in temperature corresponding to a unit change in the linewidth, which can be expressed as,

$$S_T = \frac{\Delta(\Delta\nu)}{\Delta T} \quad (12)$$

where $\Delta\nu$ represents the cavity-EIT linewidth. Similarly the sensitivity for \bar{n} can be written as,

$$S_{\bar{n}} = \frac{\Delta(\Delta\nu)}{\Delta\bar{n}} \quad (13)$$

The minimum achievable temperature of the ion, as well as the separation between the motional energy levels, is inherently determined by the secular frequency of the ion trap. This follows from the fact that the effective temperature corresponding to the ground-state energy of the phonon ladder scales with the secular frequency as $T \sim \frac{\hbar\omega_{sec}}{2k_B}$. Consequently, a higher secular frequency leads to a larger energy spacing between the motional levels and therefore to a higher equivalent temperature scale associated with these levels. The minimum detectable temperature change on the other hand depends on the minimum resolvable linewidth change dictated by the mirror reflectivity.

At higher temperatures, the sensitivity appears to be relatively low, whereas it increases at lower temperatures. To estimate the achievable sensitivity, we assume that the minimum detectable change in the cavity-EIT linewidth is 10 kHz.

We have calculated the sensitivity for both the strong and weak-coupling regimes in the presence of a large excited-state decay rate, which represents a realistic and widely encountered experimental scenario. The parameters used in our simulations are inspired by those reported in the experiments of [51] and [38], with the exception of the secular frequency of the ion. In our case, the secular frequency must exceed the decay rates of the excited state in order to satisfy the resolved sideband condition. Accordingly, the secular frequency is chosen to be approximately 15 MHz.

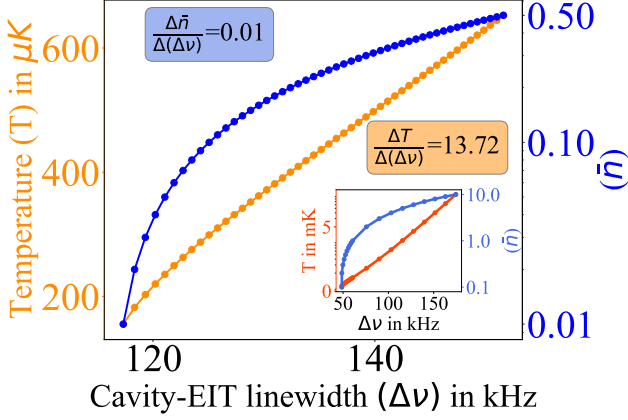


FIG. 9: Temperature vs cavity-EIT linewidth for systems operating in the strong coupling regime for a single ion. The parameters are chosen from [51]. Single ion cavity coupling $g = 12.3 \text{ MHz}$, cavity decay rate, $\kappa = 4.1 \text{ MHz}$, excited state decay, $\gamma = 12.5 \text{ MHz}$. The control field Rabi frequency (Ω_c) is taken as 3 MHz . The secular frequency is taken to be 15 MHz . The inset plot shows the variation in temperature and average phonon number over a broader range of cavity-EIT linewidth

Figure 9 represents the single-atom strong-coupling case. Typically, such conditions prevail in fiber cavity-based QED systems. From the slope of the cavity-EIT linewidth versus temperature and \bar{n} plot, we get the value of $14 \mu\text{K}/\text{kHz}$ and $0.01/\text{kHz}$, respectively. But determining 1kHz resolution in linewidth can be experimentally challenging, so if we take a minimum of 10 kHz change in linewidth, the minimum detectable temperature change will be $140 \mu\text{K}$ and the minimum detectable deviation in \bar{n} will be 0.1 . As discussed in section VII, the necessary condition for this thermometry method is to be in the resolved sideband regime ($\gamma \ll \omega_{sec}$). For this reason, the secular frequency is taken as 15 MHz , which is higher than the excited state decay rate of 12.5 MHz .

Figure 10 illustrates the sensitivity for the multi-atom low-coupling regime. About 500 atoms are considered to be coupled to the cavity, resulting in effective strong coupling. The sensitivity in this case is about $120 \mu\text{K}$ per 10 kHz change in linewidth.

The sensitivities in both cases are nearly

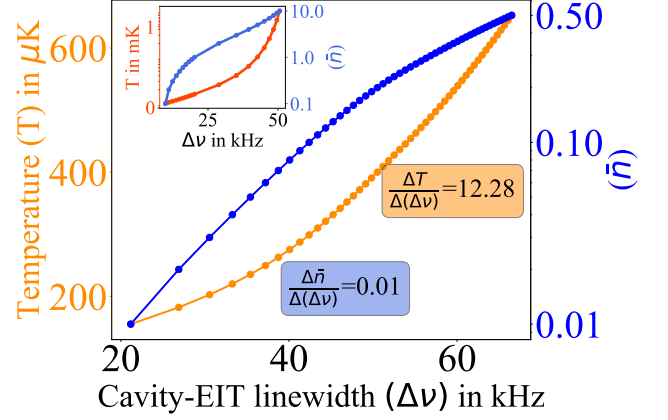


FIG. 10: Temperature vs cavity-EIT linewidth for systems operating in the weak coupling regime for a single ion. The inset plot is for a higher range of temperature, average phonon number and cavity-EIT linewidth. The parameters are chosen the same as the system given in [38]. The single ion cavity coupling factor $g = 0.54 \text{ MHz}$. The cavity decay rate is $\kappa = 2.2 \text{ MHz}$, and the excited state decay rate is $\gamma = 12.5 \text{ MHz}$. The Rabi frequency for control field (Ω_c) is 3 MHz . The secular frequency is considered as 15 MHz to maintain the resolved sideband regime.

identical, as both are in an effective strong coupling regime with a similar effective coupling factor. A similar behaviour is also observed when considering the average phonon occupation number (\bar{n}).

In our case, as represented in Figure 9 and Figure 10, the assumed secular frequency is ($\sim 15 \text{ MHz}$), which is required to satisfy the strict conditions discussed earlier. This secular frequency value is significantly higher than that used in conventional trapped-ion experiments (typically $\sim 1 \text{ MHz}$) since the analysis is performed for calcium ($^{40}\text{Ca}^+$) ion. As a result, the temperature change corresponding to a given variation in the EIT linewidth, as well as in \bar{n} , becomes larger. This reduces the temperature sensitivity of the method, although the sensitivity in terms of the average phonon occupation number \bar{n} remains unaffected.

IX. ROADMAP TOWARDS EXPERIMENTAL REALIZATION

We discuss an outline of experimental implementations for the trapped-ion thermometry method discussed in the previous sections of the article. As the thermal state detection method proposed is cavity EIT-based, one needs to engineer a trapped-ion cavity-QED system in the strong-coupling regime ($g^2 \gg \kappa\gamma$). This may be achieved in two ways. The first approach would be to engineer a cavity configuration in the near-concentric or near-confocal regime as per the requirements of the physics objectives. We recommend using a high finesse (> 50000) cavity, such that the coupling factor (g) is high enough to justify operation in the strong coupling regime ($g^2 \gg \kappa\gamma$) for a single atom/ion coupled to the cavity mode. The second approach focuses on a relatively relaxed regime of multi-ion based strong coupling regime of operation for a low-finesse cavity.

We need to choose a particular ion species with suitable energy levels, and appropriate ion trap parameters such that the system stays in the resolved sideband regime ($\gamma \ll \omega_{sec}$). Most of the ion species used in cavity-QED experiments globally typically have strong dipole-allowed transitions, with broad linewidths, where sidebands are not resolved in general. Such traps operate with typical trap frequencies in the range (ω_{sec}) $\approx 0.5 - 2MHz$. So, one needs a judicious choice of the energy levels, such that the effective three-level system realized has very narrow linewidths for one of the excited levels.

One may also consider using a dipole allowed transition (where typical linewidths are in the range of $\approx 5 - 20MHz$) for the trapped ion strongly coupled to the cavity field, one should consider operating the ion trap in a very tight confinement (very deep trap potential) of the ion with a secular frequency greater than the transition linewidth (Γ). Such a mode of ion trap operation has been experimentally validated [53], where an ${}^9Be^+$ ion was trapped with a very high RF voltage (600 V) and frequency (240

MHz), reaching secular frequencies in the range of $\sim 50 MHz$ and the sideband transitions were addressed in a dipole-allowed transition.

If one considers applying the proposed thermometry method with multiple ions in low-to medium-finesse (finesse values in the range 3000 – 15000) cavities having a relatively large mode waist (50 – 100 μm), about 10 ions coupled to the cavity mode can allow the system to operate in the strong-coupling regime, assuming a single ion cavity coupling factor of 0.5 MHz and cavity decay rate as well as the excited state decay rate of about 1 MHz.

X. CONCLUSION

We have presented a cavity-assisted thermometry scheme for trapped ions that takes advantage of the dependence of cavity-induced EIT on ions' motional state. Through the explicit integration of thermalization and vibrational sidebands into a cavity-QED Λ -type system, we show that the mean phonon occupation and the ion temperature can be directly measured by the linewidth of the cavity-EIT transparency window. By means of motion-induced dephasing, thermal phonons perturb the coherence of the EIT dark state, resulting in a systematic expansion of the cavity-EIT resonance. This enables direct extraction of the ion temperature from the measured cavity transmission spectrum, eliminating the need for projective internal-state detection in Rabi spectroscopy. Overall, for the diagnosis of ion temperature in cavity-QED systems, cavity-EIT-based thermometry provides a minimally invasive and experimentally feasible method. The established coupling between ion motion and cavity transmission goes beyond thermometry, offering a platform to investigate measurement-induced effects in cavity-QED systems and enabling continuous monitoring of motional heating

Acknowledgments

Abhijit Kundu gratefully acknowledges financial support from IIT Tirupati, Government of India. Vijay Bhatt acknowledges support from the NQM (National Quantum Mission), Department of Science and Technology, Ministry of Science and Technology, Government of India through Project No. DST/QTC/NQM/QComm/2024/2(G) administered through the IITM CDOT SAMGYNA TECHNOLOGIES FOUNDATION, IIT Madras, Chennai, Tamil Nadu

- 600113. Arijit Sharma acknowledges support from the NQM (National Quantum Mission), Department of Science and Technology, Ministry of Science and Technology, Government of India through Project Nos. DST/QTC/NQM/QComm/2024/2(G) and DST/QTC/NQM/QComm/2024/2(C) administered through the IITM CDOT SAMGYNA TECHNOLOGIES FOUNDATION, IIT Madras, Chennai, Tamil Nadu - 600113.

Conflicts of Interest

The authors declare no conflicts of interest.

-
- [1] D. Leibfried, R. Blatt, C. Monroe, and D. Wineland, Quantum dynamics of single trapped ions, *Rev. Mod. Phys.* **75**, 281 (2003).
- [2] H. Häffner, C. F. Roos, and R. Blatt, Quantum computing with trapped ions, *Phys. Rep.* **469**, 155 (2008).
- [3] C. Monroe and J. Kim, Scaling the ion trap quantum processor, *Science* **339**, 1164 (2013).
- [4] D. Fang, W.-B. Chen, C.-H. Zhang, J.-M. Cui, Y.-F. Huang, C.-F. Li, and G.-C. Guo, Cavity-assisted thermometry for a single trapped ion, *Phys. Rev. Appl.* **24**, 024037 (2025).
- [5] F. Diedrich, J. C. Bergquist, W. M. Itano, and D. J. Wineland, Laser cooling to the zero-point energy of motion, *Phys. Rev. Lett.* **62**, 403 (1989).
- [6] C. F. Roos, D. Leibfried, A. B. Mundt, F. Schmidt-Kaler, J. Eschner, and R. Blatt, Experimental demonstration of ground state laser cooling with electromagnetically induced transparency, *Phys. Rev. Lett.* **85**, 5547 (2000).
- [7] D. J. Wineland, C. Monroe, W. M. Itano, D. Leibfried, B. E. King, and D. M. Meekhof, Experimental issues in coherent quantum-state manipulation of trapped atomic ions, *J. Res. Natl. Inst. Stand. Technol.* **103**, 259 (1998).
- [8] M. Brownnutt, M. Kumph, P. Rabl, and R. Blatt, Ion-trap measurements of electric-field noise near surfaces, *Rev. Mod. Phys.* **87**, 1419 (2015).
- [9] J. I. Cirac and P. Zoller, Quantum computations with cold trapped ions, *Physical review letters* **74**, 4091 (1995).
- [10] R. Blatt and D. Wineland, Entangled states of trapped atomic ions, *Nature* **453**, 1008 (2008).
- [11] Q. A. Turchette, D. Kielpinski, B. E. King, D. Leibfried, D. M. Meekhof, C. J. Myatt, M. A. Rowe, C. A. Sackett, C. S. Wood, W. M. Itano, C. Monroe, and D. J. Wineland, Heating of trapped ions from the quantum ground state, *Phys. Rev. A* **61**, 063418 (2000).
- [12] H. J. Kimble, The quantum internet, *Nature* **453**, 1023 (2008).
- [13] D. M. Meekhof, C. Monroe, B. E. King, W. M. Itano, and D. J. Wineland, Generation of nonclassical motional states of a trapped atom, *Phys. Rev. Lett.* **76**, 1796 (1996).
- [14] C. Roos, T. Zeiger, H. Rohde, H. C. Nägerl, J. Eschner, D. Leibfried, F. Schmidt-Kaler, and R. Blatt, Quantum state engineering on an optical transition and decoherence in a paul trap, *Phys. Rev. Lett.* **83**, 4713 (1999).
- [15] A. J. Rasmusson, M. D'Onofrio, Y. Xie, J. Cui, and P. Richerme, Optimized pulsed sideband cooling and enhanced thermometry of trapped ions, *Phys. Rev. A* **104**, 043108 (2021).
- [16] I. Vybornyi, L. S. Dreissen, D. Kiesenhofer, H. Hainzer, M. Bock, T. Ollikainen, D. Vadlejch, C. F. Roos, T. E. Mehlstäubler, and K. Hammerer, Sideband thermometry of ion crystals, *PRX Quantum* **4**, 040346 (2023).
- [17] H. J. Kimble, Strong interactions of single atoms and photons in cavity QED, *Phys. Scr.* **1998**, 127 (1998).
- [18] M. Brune, F. Schmidt-Kaler, A. Maali, J. Dreyer, E. Hagley, J. Raimond, and S. Haroche, Quantum Rabi oscillation: a direct test of field quantization in a cavity, *Phys. Rev. Lett.* **76**, 1800 (1996).
- [19] A. Reiserer and G. Rempe, Cavity-based quantum networks with single atoms and optical photons, *Rev. Mod. Phys.* **87**, 1379 (2015).
- [20] V. M. Acosta, K. Jensen, C. Santori, D. Budker, and R. G. Beausoleil, Electromagnetically induced transparency in a diamond spin ensemble enables all-optical electromagnetic field sensing, *Phys. Rev. Lett.* **110**, 213605 (2013).
- [21] H. Wang, D. Goorskey, W. Burkett, and M. Xiao, Cavity-linewidth narrowing by means of electromagnetically induced transparency, *Opt. Lett.* **25**, 1732 (2000).
- [22] M. J. Werner and A. Imamoglu, Photon-photon interactions in cavity electromagnetically induced transparency, *Phys. Rev. A* **61**, 011801 (1999).
- [23] M. Mücke, E. Figueroa, J. Bochmann, C. Hahn, K. Murr, S. Ritter, C. J. Villas-Boas, and G. Rempe, Electromagnetically induced transparency with single atoms in a cavity, *Nature* **465**, 755 (2010).
- [24] H. Tanji-Suzuki, W. Chen, R. Landig, J. Simon, and V. Vuletić, Vacuum-induced transparency, *Science* **333**, 1266 (2011).

- [25] L.-M. Duan and C. Monroe, Colloquium: Quantum networks with trapped ions, *Rev. Mod. Phys.* **82**, 1209 (2010).
- [26] A. Reiserer, Colloquium: Cavity-enhanced quantum network nodes, *Rev. Mod. Phys.* **94**, 041003 (2022).
- [27] K.-J. Boller, A. Imamoglu, and S. E. Harris, Observation of electromagnetically induced transparency, *Phys. Rev. Lett.* **66**, 2593 (1991).
- [28] I. Novikova, R. L. Walsworth, and Y. Xiao, Electromagnetically induced transparency-based slow and stored light in warm atoms, *Laser Photonics Rev.* **6**, 333 (2012).
- [29] L. Ma, O. Slattery, and X. Tang, Optical quantum memory based on electromagnetically induced transparency, *J. Opt.* **19**, 043001 (2017).
- [30] G. Morigi, J. Eschner, and C. H. Keitel, Ground state laser cooling using electromagnetically induced transparency, *Phys. Rev. Lett.* **85**, 4458 (2000).
- [31] J. Souza, E. Figueroa, H. Chibani, C. Villas-Boas, and G. Rempe, Coherent control of quantum fluctuations using cavity electromagnetically induced transparency, *Phys. Rev. Lett.* **111**, 113602 (2013).
- [32] J. I. Cirac, R. Blatt, P. Zoller, and W. D. Phillips, Laser cooling of trapped ions in a standing wave, *Phys. Rev. A* **46**, 2668 (1992).
- [33] J. Roßnagel, K. N. Tolazzi, F. Schmidt-Kaler, and K. Singer, Fast thermometry for trapped ions using dark resonances, *New Journal of Physics* **17**, 045004 (2015).
- [34] B. Norton, E. Streed, M. Petrasiumas, A. Jechow, and D. Kielpinski, Millikelvin spatial thermometry of trapped ions, *New Journal of Physics* **13**, 113022 (2011).
- [35] M. D. Lukin, M. Fleischhauer, M. O. Scully, and V. L. Velichansky, Intracavity electromagnetically induced transparency, *Opt. Lett.* **23**, 295 (1998).
- [36] H. Wu, J. Gea-Banacloche, and M. Xiao, Observation of intracavity electromagnetically induced transparency and polariton resonances in a doppler-broadened medium, *Phys. Rev. Lett.* **100**, 173602 (2008).
- [37] J. Zhang, G. Hernandez, and Y. Zhu, Slow light with cavity electromagnetically induced transparency, *Opt. Lett.* **33**, 46 (2007).
- [38] M. Albert, A. Dantan, and M. Drewsen, Cavity electromagnetically induced transparency and all-optical switching using ion coulomb crystals, *Nat. Photon.* **5**, 633 (2011).
- [39] Y.-C. Liu, B.-B. Li, and Y.-F. Xiao, Electromagnetically induced transparency in optical microcavities, *Nanophotonics* **6**, 789 (2017).
- [40] S. Zhang, Z.-P. Huang, T.-C. Tian, Z.-Y. Wu, J.-Q. Zhang, W.-S. Bao, and C. Guo, Sideband cooling of a trapped ion in strong sideband coupling regime, *Opt. Express* **31**, 44501 (2023).
- [41] D. Manzano, A short introduction to the Lindblad master equation, *AIP Adv.* **10**, 025106 (2020).
- [42] L. R. S. Santos, M. H. Oliveira, L. O. R. Solak, D. Z. Rossatto, and C. J. Villas-Boas, Fundamental limit to cavity linewidth narrowing with single atoms (2024), arXiv:2411.12422 [quant-ph].
- [43] M. Fleischhauer, A. Imamoglu, and J. P. Marangos, Electromagnetically induced transparency: Optics in coherent media, *Rev. Mod. Phys.* **77**, 633 (2005).
- [44] M. Lukin, Colloquium: Trapping and manipulating photon states in atomic ensembles, *Rev. Mod. Phys.* **75**, 457 (2003).
- [45] A. Dantan and M. Pinard, Quantum-state transfer between fields and atoms in electromagnetically induced transparency, *Physical Review A—Atomic, Molecular, and Optical Physics* **69**, 043810 (2004).
- [46] M. Mücke, E. Figueroa, J. Bochmann, C. Hahn, K. Murr, S. Ritter, C. J. Villas-Boas, and G. Rempe, Electromagnetically induced transparency with single atoms in a cavity, *Nature* **465**, 755 (2010).
- [47] M. Mücke, *Elektromagnetisch induzierte Transparenz mit einem einzelnen Atom*, Ph.D. thesis, Technische Universität München (2011).
- [48] A. Sørensen and K. Mølmer, Entanglement and quantum computation with ions in thermal motion, *Physical Review A* **62**, 022311 (2000).
- [49] D. J. Wineland and W. M. Itano, Laser cooling of atoms, *Phys. Rev. A* **20**, 1521 (1979).
- [50] J. Schupp, V. Krucmarskiy, V. Krutyanskiy, M. Meraner, T. Northup, and B. Lanyon, Interface between trapped-ion qubits and traveling photons with close-to-optimal efficiency, *PRX Quantum* **2**, 020331 (2021).
- [51] H. Takahashi, E. Kassa, C. Christoforou, and M. Keller, Strong coupling of a single ion to an optical cavity, *Phys. Rev. Lett.* **124**, 013602 (2020).
- [52] M. Albert, J. P. Marler, P. F. Herskind, A. Dantan, and M. Drewsen, Collective strong coupling between ion coulomb crystals and an optical cavity field: Theory and experiment, *Phys. Rev. A* **85**, 023818 (2012).
- [53] S. R. Jefferts, C. Monroe, E. W. Bell, and D. J. Wineland, Coaxial-resonator-driven rf (Paul) trap for strong confinement, *Phys. Rev. A* **51**, 3112 (1995).
- [54] M. Albert, *A light-matter interface based on ion Coulomb crystals in an optical cavity*, Ph.D. thesis, Danish National Research Foundation, Center for Quantum Optics - QUANTOP, Department of Physics and Astronomy, The University of Aarhus (2010).
- [55] E. Peik, J. Abel, T. Becker, J. von Zanthier, and H. Walther, Sideband cooling of ions in radio-frequency traps, *Phys. Rev. A* **60**, 439 (1999).

Appendix A: Transmission and reflection spectra with a bare cavity

To validate the theoretical model and numerical simulations discussed in the earlier sections of the article, we examine the empty-cavity limit by setting the ion-cavity coupling strength to zero and ignoring all phonon-related contributions in the Hamiltonian. Under these conditions, the system reduces to a driven, dissipative optical cavity described solely by the bare cavity Hamiltonian and the decay channels associated with it.

The Hamiltonian of the bare cavity system can be expressed as,

$$H_{\text{bare}} = \Delta_c a^\dagger a + i\sqrt{2\kappa_1}(a^\dagger a_{\text{in}} - a_{\text{in}}^\dagger a), \quad (\text{A1})$$

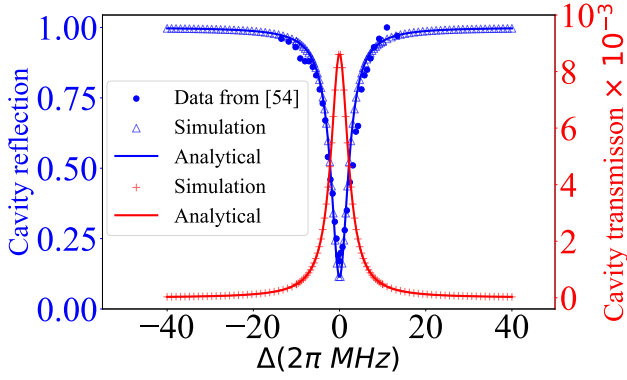


FIG. 11: Cavity reflection from simulation, analytical expression and published experimental data [54] as a function of probe detuning. The free spectral range of the cavity is $\nu_{FSR} = 12.7$ GHz. The transmission coefficients of the mirrors are $T_1 = 1500$ ppm and $T_2 = 5$ ppm, while the intracavity loss coefficient is $A = 600$ ppm. For these parameters, the resulting cavity finesse is approximately $F \sim 3000$.

where a^\dagger (a) is the creation (annihilation) operator for the cavity mode, Δ_c represents the probe-cavity detuning, and a_{in} is the input field injected into the cavity.

Standard input-output relations are used to calculate the resulting transmission (\mathcal{T}) and reflection (\mathcal{R}) spectra. For an empty cavity, the response follows the well-known Lorentzian resonance profile determined by the cavity decay rates.

$$\mathcal{R} = \left| \frac{a_{\text{ref}}}{a_{\text{in}}} \right|^2 = \frac{(\kappa - 2\kappa_1)^2 + \Delta_c^2}{\kappa^2 + \Delta_c^2}, \quad (\text{A2})$$

$$\mathcal{T} = \left| \frac{a_{\text{trans}}}{a_{\text{in}}} \right|^2 = \frac{4\kappa_1\kappa_2}{\kappa^2 + \Delta_c^2}, \quad (\text{A3})$$

where, κ corresponds to the total decay rate of the cavity field, while κ_1 and κ_2 represent the contribution to the cavity loss arising from the imperfect reflectivity of the two cavity mirrors.

Figure 11 shows the cavity transmission and reflection spectra obtained from our numerical simulation together with the corresponding analytical expression and previously reported experimental data [54]. The obtained spectra exhibit the expected Lorentzian lineshape with

normalization, reproducing the well-known analytical response of a bare cavity. The validity of the reduced Hamiltonian reflecting the response of the bare cavity and the numerical method used throughout the manuscript are confirmed by the excellent agreement with the standard bare-cavity reflection and transmission profiles. The bare cavity response therefore serves as a baseline reference against which the modifications arising from ion-cavity interactions and phonon-induced effects can be reliably identified in the main results.

Appendix B: Comparison of simulation results with analytical expressions and experimental data

We verify our numerical simulations for a multi-ion cavity-QED system exhibiting a low single-ion cavity coupling factor as well as using ions with a large decay rate of the excited state. These systems can be driven in the collective strong coupling regime by appropriate choice of ions coupled to the cavity mode. We compare the simulated normalized cavity emission spectrum with previously published experimental data and results and compare them with available analytical expressions mentioned in [47, 54].

We first consider the cavity-EIT model described in [47], where a three-level Λ -type atom interacts with a single mode of an optical cavity. The atomic system consists of an excited state $|e\rangle$ and two long-lived ground states $|g\rangle$ and $|u\rangle$. The cavity mode is coupled to the transition $|g\rangle \leftrightarrow |e\rangle$ with coupling strength g while a classical control field with Rabi frequency Ω_c drives the transition $|u\rangle \leftrightarrow |e\rangle$. The cavity mode is driven by a weak probe field with amplitude ϵ and the cavity output spectrum is measured as a function of the probe-cavity detuning. In the rotating frame, the system Hamiltonian can be expressed as,

$$H = \hbar \left[\Delta_1 \sigma_{ee} + (\Delta_1 - \Delta_2) \sigma_{uu} + g(a^\dagger \sigma_{ge} + \sigma_{eg} a) + \frac{\Omega_c}{2} (\sigma_{ue} + \sigma_{eu}) + \epsilon (a^\dagger + a) - \Delta a^\dagger a \right], \quad (\text{B1})$$

where detunings are defined as $\Delta_1 = \omega_{eg} - \omega_p$, $\Delta_2 = \omega_{eu} - \omega_c$ and $\Delta = \omega_c - \omega_p$. ω_p and ω_c correspond to the probe and control field frequencies, respectively.

The intracavity photon number can be obtained analytically from the steady-state cavity field in the weak-probe limit as,

$$\langle n \rangle = \langle a^\dagger a \rangle = \frac{|\epsilon|^2}{|(\Delta + i\kappa) - \chi|^2}, \quad (\text{B2})$$

where κ represents the cavity decay rate and χ is the effective susceptibility of the EIT medium,

$$\chi = \frac{g^2 N (\Delta - \Delta_1 + \Delta_2 + i\gamma_{u,\text{deph}})}{(\Delta - \Delta_1 + i(\gamma_{eg} + \gamma_{eu}))} \times \frac{1}{(\Delta - \Delta_1 + \Delta_2 + i\gamma_{u,\text{deph}}) - \Omega_c^2/4}. \quad (\text{B3})$$

With these analytical expression and the parameters listed in [47] we compute the transmission spectrum and compared it with the outcomes of our numerical model. Figure 12 highlighted the normalized cavity emission as a function of probe detuning (Δ/κ) having $N_{\text{ions}} = 17$. As observed, the simulation accurately reproduces the key spectral features, including the central transparency peak and two sidebands.

The accuracy of the theoretical implementation is confirmed by the excellent agreement between the simulations and the analytical prediction. Furthermore, the close overlap with experimental data confirms the physical assumptions incorporated in the model. This agreement shows that the numerical framework reproduces experimentally observed behavior with high reliability and captures the cavity-EIT dynamics.

To further validate our numerical model, we also compare our results with the reflection spectra published in [54]. This work examines the cavity reflection from an ensemble of atoms

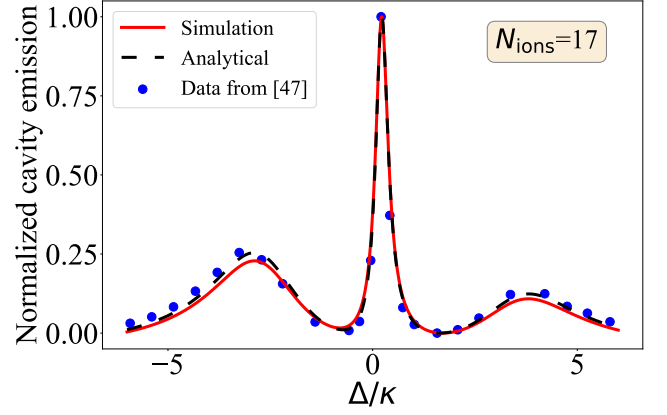


FIG. 12: Normalized cavity emission from simulation, analytical expression and published experimental data [47] as a function of probe detuning. The cavity decay rate (κ), is 1 MHz, while the single-atom cavity coupling rate (g_0) is 0.7κ . The control field Rabi frequency (Ω_c) is $3MHz$. The detuning for probe laser (Δ_1) and control laser (Δ_2) are 0.8κ and 0.55κ respectively.

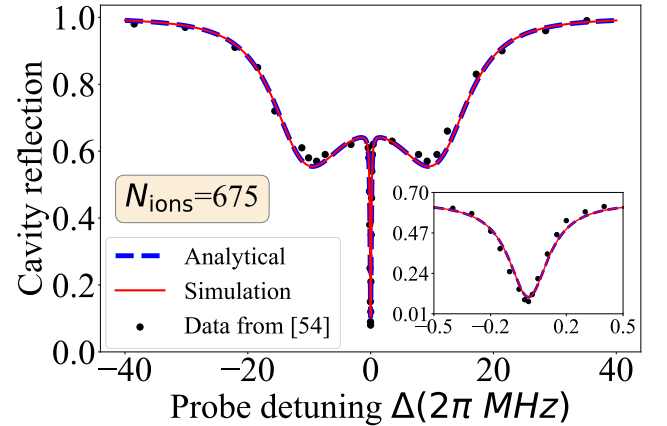


FIG. 13: Cavity reflection from simulation, analytical expression and published experimental data [54] as a function of probe detuning. The decay rate for 1st mirror (κ_1), 2nd mirror (κ_2) are $1.6MHz$ and $0.5kHz$ respectively. The decay rates from excited state to first and 2nd ground state are, $\gamma_{31} = 12.6 MHz$ and $\gamma_{21} = 0.6 kHz$ respectively. The single atom coupling factor $g = 0.48 MHz$, while control field Rabi frequency, $\Omega_c = 4.1 MHz$.

coupled to the cavity mode in contrast to the previous work in [47], which concentrates on the cavity transmission spectrum. Specifically, for the system of about 500 atoms, the reflection spectrum was investigated analytically and experimentally in [54].

The cavity-EIT spectrum shown in Figure 13 is deduced from the analytical expression of the normalized cavity reflectivity with respect to the input field, as explained in [54]. The reflectivity can be written as,

$$R = \left| \frac{a_{ref}}{a_{in}} \right|^2 = \frac{[\kappa_1 - \kappa_2 - \kappa_A - \text{Im}(\chi_\Lambda)]^2 + [\Delta - \text{Re}(\chi_\Lambda)]^2}{\kappa^2 + \Delta^2 + |\chi_\Lambda|^2 + 2[\kappa \text{Im}(\chi_\Lambda) - \Delta \text{Re}(\chi_\Lambda)]} \quad (\text{B4})$$

Here a_{ref} and a_{in} are the reflected and input field amplitude respectively. κ_1 , κ_2 and κ_A are the decay rates for field losses from the cavity first mirror, second mirror and additional internal losses due to various mechanisms. Δ is the probe field detuning and κ is the total decay rate ($\kappa = \kappa_1 + \kappa_2 + \kappa_A$). χ_Λ is the three-level non-linear susceptibility of the atomic ensemble, which can be expressed as,

$$\chi_\Lambda = \frac{ig^2N}{\gamma + i\Delta} \frac{\ln(1+s)}{s} \quad (\text{B5})$$

Where, g is the single ion coupling factor, N is the effective number of atoms coupled with the cavity field, γ is the combined decay rates for the excited state. The saturation parameter for the two-photon transition is s , which can be articulated as,

$$s = \frac{\Omega_c^2/2}{(\gamma_{12} + i\delta)(\gamma + i\Delta)} \quad (\text{B6})$$

Where, Ω_c , is the control field Rabi frequency, γ_{12} is the dephasing rate between the ground states. δ is the two-photon detuning, which is the difference between probe laser detuning (Δ) and control laser detuning (Δ_{32}), $\delta = \Delta - \Delta_{32}$.

Appendix C: Dependency of cavity-EIT linewidth on cavity coupling parameter g and control field Rabi frequency Ω_c for different n_{th}

A two-dimensional map of the cavity-EIT linewidth represented as the normalized full width at half maxima (FWHM) ratio as a function of the normalized control field Rabi

frequency Ω_c and the normalized atom-cavity coupling strength g for various mean thermal phonon numbers n_{th} is shown in Figure 14. For a weakly excited motional state ($n_{th} = 0.5$) (see Figure 14a), the linewidth ratio remains close to unity over a large region of the parameter space. This suggests that thermal motion only slightly alters EIT coherence. As the value of thermal occupation increases $n_{th} = 1$ (see Figure 14b), a clear reduction of the FWHM ratio occurs, particularly in the regime of strong ion-cavity coupling and weak control fields. This reduction signals the onset of thermally induced decoherence. A higher phonon number ($n_{th} = 5, 10$) (see Figure 14c, Figure 14d) shows a more noticeable trend in which the parameter space is dominated by extended regions of reduced linewidth ratio. In this regime, thermal motion significantly perturbs the ion-cavity interaction, leading to enhanced dephasing and a degradation of the EIT interference. As the control-field strength in-

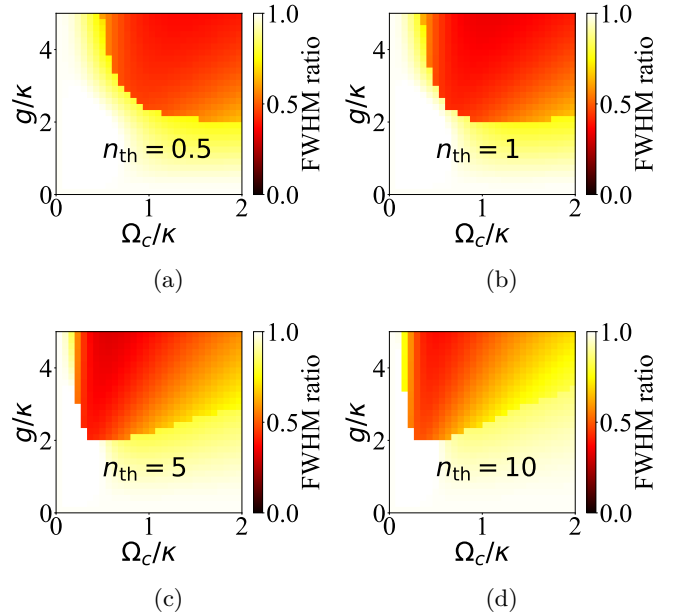


FIG. 14: Two-dimensional maps of the cavity-EIT linewidth as a function of the atom-cavity coupling strength g and the coupling-laser Rabi frequency Ω_c for different mean thermal phonon numbers \bar{n}_{th} .

creases, it partially mitigates this effect by stabilizing the dark state against motional fluctuations. The strong sensitivity of the cavity response to the ions' motional state is highlighted by the systematic and temperature-dependent

modification of the cavity-EIT linewidth shown in these plots. This provides a solid foundation for thermometry using cavity-based EIT.

Appendix D: Verification of different sideband transition -related phenomenon

As proof of principle of our approach, we performed verification of different sideband transition related characteristics. In the case of sideband transitions, a two-level system dressed with vibrational levels is sufficient to address different properties. The sideband Hamiltonians used here are consistent with the Lamb–Dicke-expanded interaction employed in the main text. The two kinds of sideband transitions (BSB and RSB) are described by the Hamiltonian which is similar to the 4th term (with the multiplication of the Lamb-Dicke parameter η) of Equation 10 with the reduced Hilbert space of only photon and phonon. The Hamiltonian for blue and red sideband transition can be written as [1],

$$\begin{aligned} H_{BSB} &= \eta\Omega_c (\sigma_{eu}b^\dagger + \sigma_{ue}b) \\ H_{RSB} &= \eta\Omega_c (\sigma_{eu}b + \sigma_{ue}b^\dagger) \end{aligned} \quad (D1)$$

For a thermal distribution of ion the strengths of red and blue sideband transitions are unequal and depends on the phonon number (n). The probability of occupying the excited state for RSB and BSB transition is related by the formula [11],

$$\frac{P_{RSB}}{P_{BSB}} = \frac{n}{n+1} \quad (D2)$$

We verified this principle for a range of phonon numbers and different Lamb-Dicke parameters. In Figure 15, the comparison between the probability ratio from simulation and phonon ratio from Equation D2 has been shown for four different Lamb-Dicke parameters. At lower values of Lamb-Dicke parameters, these two quantities are well-matched, which consistent with the theory. For higher Lamb-Dicke parameters the simulation result and theory start to deviate as the boundary of the Lamb-Dicke regime ($\eta \ll 1$) is approached, whereas sideband transitions as-

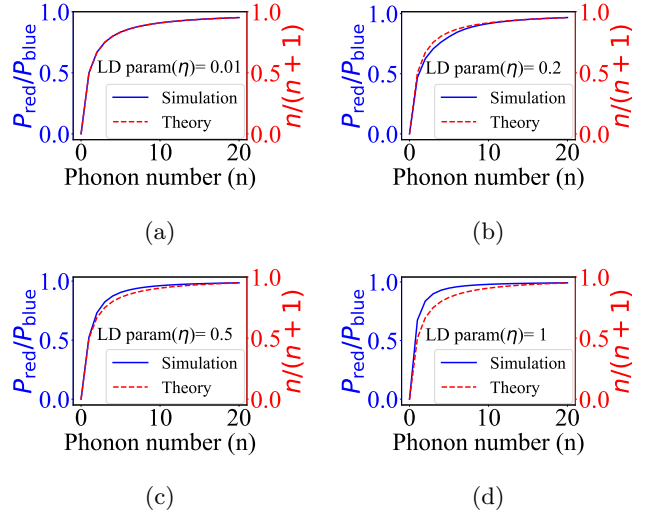


FIG. 15: Ratio of excited state occupation probability for blue and red sideband transition is compared with phonon number ratio. Plots (a)–(d) correspond to increasing values of the Lamb–Dicke parameter η .

sume that the ion is well within the Lamb-Dicke regime.

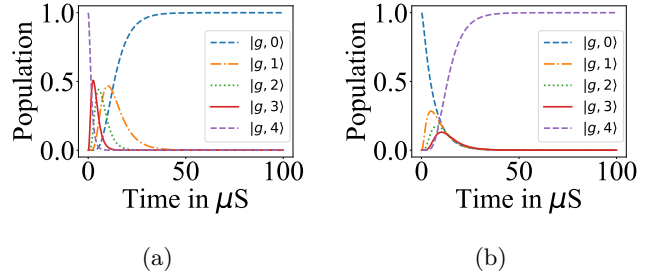


FIG. 16: Simulated state evolution with time. The simulation runs with Lamb-Dicke parameter, $\eta = 0.2$, Rabi frequency, $\Omega = 2MHz$, and excited state decay rate, $\gamma = 2\Omega$. (a) Time evolution of different states in red sideband transition. The initial state is taken as $|g, 5\rangle$, after applying sequential RSB pulses, phonon number decreases, and finally the system reaches the ground state, $|g, 0\rangle$. (b) Time evolution for blue sideband transition. population goes from initial $|g, 0\rangle$ to higher phonon state $|g, 5\rangle$.

A larger application of the sideband transition is the cooling of the atom to its motional ground state [5, 55]. When the resolved sideband regime is obtained ($\gamma \ll \omega_{sec}$) and the laser is tuned to a RSB transition, the atom loses one quanta of energy upon excitation ($|g, n\rangle \rightarrow |e, n-1\rangle$). From the excited state, there is a high chance that it spontaneously decays to the ground state with

the same motional quanta ($|g, n - 1\rangle$). Thus, a motional quanta has been reduced in this process. By repeating this process multiple times, the vibrational quanta has been reduced in each steps and eventually we reached to the ground

state of the atom (see Figure 16a). Similarly, if the laser is tuned to the BSB transition, starting from a ground state, the atom lands in a higher phonon state depending on the number of sideband pulses applied (see Figure 16b).